

# Discovery of a Be/X-ray pulsar binary and associated supernova remnant in the Wing of the SMC

V. Hénault-Brunet<sup>1</sup>★, L. M. Oskinova<sup>2</sup>, M. A. Guerrero<sup>3</sup>, W. Sun<sup>4</sup>, Y.-H. Chu<sup>5</sup>,  
C. J. Evans<sup>6,1</sup>, J. S. Gallagher III<sup>7</sup>, R. A. Gruendl<sup>5</sup>, J. Reyes-Iturbide<sup>8</sup>

<sup>1</sup>Scottish Universities Physics Alliance (SUPA), Institute for Astronomy, University of Edinburgh, Blackford Hill, Edinburgh, EH9 3HJ, UK

<sup>2</sup>Institute for Physics and Astronomy, University of Potsdam, 14476 Potsdam, Germany

<sup>3</sup>Instituto de Astrofísica de Andalucía, IAA-CSIC. c/ Glorieta de la Astronomía s/n, 18008 Granada, Spain

<sup>4</sup>Department of Astronomy, Nanjing University, Nanjing, 210093 Jiangsu, China

<sup>5</sup>Department of Astronomy, University of Illinois, 1002 West Green Street, Urbana, IL 61801, USA

<sup>6</sup>UK Astronomy Technology Centre, Royal Observatory Edinburgh, Blackford Hill, Edinburgh, EH9 3HJ, UK

<sup>7</sup>Department of Astronomy, University of Wisconsin-Madison, 5534 Sterling, 475 North Charter St., Madison, WI 53706, USA

<sup>8</sup>Escuela Superior de Física y Matemáticas, IPN, U.P. Adolfo López Mateos, C.P. 07738 D.F., Mexico

Accepted 2011 October 27. Received 2011 October 27; in original form 2011 October 12

## ABSTRACT

We report on a new Be/X-ray pulsar binary located in the Wing of the Small Magellanic Cloud (SMC). The strong pulsed X-ray source was discovered with the *Chandra* and *XMM-Newton* X-ray observatories. The X-ray pulse period of 1062 s is consistently determined from both *Chandra* and *XMM-Newton* observations, revealing one of the slowest rotating X-ray pulsars known in the SMC. The optical counterpart of the X-ray source is the emission-line star 2dFS 3831. Its B0-0.5(III)e+ spectral type is determined from VLT-FLAMES and 2dF optical spectroscopy, establishing the system as a Be/X-ray binary (Be-XRB). The hard X-ray spectrum is well fitted by a power-law with additional thermal and blackbody components, the latter reminiscent of persistent Be-XRBs. This system is the first evidence of a recent supernova in the low density surroundings of NGC 602. We detect a shell nebula around 2dFS 3831 in H $\alpha$  and [O III] images and conclude that it is most likely a supernova remnant. If it is linked to the supernova explosion that created this new X-ray pulsar, its kinematic age of  $(2 - 4) \times 10^4$  yr provides a constraint on the age of the pulsar.

**Key words:** X-rays: binaries – stars: emission-line, Be – Magellanic Clouds.

## 1 INTRODUCTION

The Small Magellanic Cloud (SMC) is host to a large population of  $\sim 50$  high-mass X-ray binaries (HMXBs), comparable to the number known in the Galaxy (e.g. Haberl & Pietsch 2004; Coe et al. 2005; Reig 2011). However, unlike the Galactic population, all of these systems but one are Be/X-ray binary (Be-XRB) systems, with the exception (SMC-X1) containing a supergiant companion instead (Webster et al. 1972).

The Wing of the SMC is the region linking the eastern side of the SMC to the Bridge. Despite its lower content of gas, dust, and stars, it had a major star forming event  $\sim 11$  Myr ago and appears, as expected, deficient in Be-XRBs (Antoniou et al. 2010). Note however that the coverage of the SMC Wing by X-ray observations has been sparser than that of the Bar. Each new discovery of a Be-XRB in the SMC Wing is therefore particularly noteworthy (e.g. McGowan et al. 2007).

We have conducted *Chandra* and *XMM-Newton* observations

of the far eastern region of the Wing, concentrating on the star forming region NGC 602. The full description of these observations will be presented in a forthcoming paper (Oskinova et al., in preparation). In this letter, we concentrate on one bright X-ray source located near NGC 602 in projection and coinciding with the emission-line star 2dFS 3831 (R.A. =  $1^{\text{h}}27^{\text{m}}46.03^{\text{s}}$ , Dec. =  $-73^{\circ}32'56.42''$ , J2000.0), which is revealed as a Be-XRB. Based on the results of section 2.2, throughout this paper we will refer to the X-ray source as SXP 1062 following the nomenclature of Coe et al. (2005) for SMC X-ray pulsars.

The stellar population of NGC 602 (which comprises three star clusters: NGC602 A, B, and C) has been studied in detail. In addition to very old stars of 6-8 Gyr, likely the SMC field population, the NGC 602 clusters contains young stars of  $\sim 4$ -5 Myr (Westerlund 1964; Hutchings et al. 1991; Cignoni et al. 2009). The significant number of young stellar objects detected in the NGC 602A cluster (Carlson et al. 2007; Gouliermis et al. 2007) suggests that star formation is still ongoing. As for what initially triggered the formation of these clusters, the low density environment in the Wing of the SMC hints at an additional mechanism

★ E-mail: vhb@roe.ac.uk

acting along with gravitational collapse. NGC 602 is located at the intersection of three H I shells, and Nigra et al. (2008) suggested that its formation is the result of the interaction of two expanding shells  $\sim 7$  Myr ago. Schmalzl et al. (2008) proposed instead that star formation was possibly induced by encounters with the Large Magellanic Cloud or the Milky Way. NGC 602 is associated with SGS-SMC1, the only H $\alpha$  supergiant shell known in the SMC. The discovery of a Be-XRB in this area (only  $\sim 7'$  to the west of NGC 602A) provides important clues to the star formation history in the Wing and the evolution of large-scale structures in the interstellar medium.

This letter is organized as follows. We describe the X-ray observations and analysis in section 2. In section 3, we present the spectroscopy of the optical counterpart. We discuss the properties and environment of SXP 1062 in section 4 and present our conclusions in section 5.

## 2 X-RAY OBSERVATIONS

The X-ray data were obtained with the ACIS-I camera on the *Chandra* X-ray Observatory and with the EPIC cameras onboard *XMM-Newton*. The *Chandra* observations consisted of 11 separate exposures acquired between 2010-03-31 and 2010-04-29 (effective exposure time of 290.7 ks), while 4 separate exposures were obtained with *XMM-Newton* between 2010-03-25 and 2010-04-12 (EPIC-pn effective exposure time of 162.5 ks). The data were reduced using the most up-to-date versions of the corresponding data reduction software. The X-ray source CXO J012745.97-733256.5 (=SXP 1062) coinciding with the optical emission-line star 2dFS 3831 is detected in each of these 15 exposures. In the *Chandra* observations, the positional uncertainty ( $1\sigma$ ) of the X-ray source is  $0.9''$ . The source was also detected during an *XMM-Newton* slew on 2009-11-16. Interestingly, the source was not detected in the *ROSAT All Sky Survey*, although at its present luminosity it would have been bright enough at an expected *ROSAT* PSPC count rate of  $0.01 \text{ counts s}^{-1}$ .

### 2.1 Spectral analysis

Figure 1 shows the combined background-subtracted *Chandra* and *XMM-Newton* spectra of SXP 1062. The *Chandra* spectra were extracted from a  $12''.8$  circular region and the background was extracted from a concentric annular region of radii  $12''.8$  and  $19''.2$  which was free of sources. Likewise, the *XMM-Newton* spectra were extracted from a  $32''$  circular region and the background from 4 adjacent circular regions free of sources with radius  $45''$ .

As a first step the background-subtracted *Chandra* and *XMM-Newton* spectra of SXP 1062 were simultaneously fitted using a simple absorbed power-law model. The best-fit parameters, listed in Table 1, imply an absorbed flux in the energy range 0.2–12.0 keV of  $f_X = 1.8 \times 10^{-12} \text{ erg cm}^{-2} \text{ s}^{-1}$ . This corresponds to an intrinsic X-ray luminosity in this same energy range of  $L_X = 6.9 \times 10^{35} \text{ erg s}^{-1}$  assuming a distance modulus of 18.7 appropriate for the Wing (e.g. Cignoni et al. 2009), or  $L_X = 8.2 \times 10^{35} \text{ erg s}^{-1}$  for the ‘standard’ SMC distance modulus of 18.9 (e.g. Harries et al. 2003). The photon index  $\Gamma$  of  $\sim 0.75$  is typical of X-ray pulsar binaries (e.g. Yokogawa et al. 2003) and a signature of accretion onto a strongly magnetized neutron star.

The simple power-law model suggests some emission excess below 1 keV and at high energies. As a next step, we added a blackbody component, which statistically improved the fit (see Table 1).

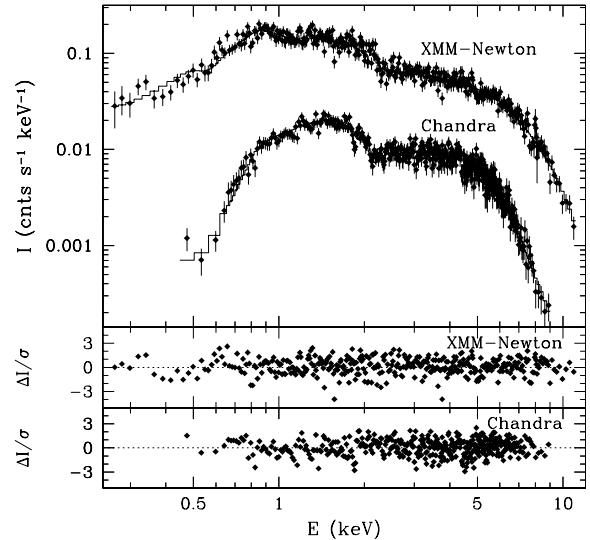


**Figure 1.** *Chandra* ACIS-I and *XMM-Newton* EPIC-pn spectra of SXP 1062. Overplotted is the best-fit model including power-law, thermal, and blackbody components. The lower panels show the residuals of the fit.

The observed X-ray flux is similar to that of the previous model, but the X-ray luminosity decreases by  $\sim 10\%$ . We also tried a model for which a thermal plasma component with SMC abundances is included instead of a blackbody. Similarly to the blackbody, the addition of a thermal component to the power-law model improves the fit. In this case, the intrinsic X-ray luminosity is only marginally greater by  $\sim 1\%$  compared to the simple power-law model.

Finally, the best fit is achieved by adding simultaneously a thermal and a blackbody component to the power-law (see Table 1 and Figure 1). The flux for this model (PBT in Table 1) is  $f_X = 1.66^{+0.19}_{-0.25} \times 10^{-12} \text{ erg cm}^{-2} \text{ s}^{-1}$ , corresponding to an intrinsic luminosity  $L_X = 6.3^{+0.7}_{-0.8} \times 10^{35} \text{ erg s}^{-1}$  for a distance modulus of 18.7.

The column densities are well constrained by spectral fitting, albeit the values slightly differ depending on the model. Using the best-fit values, we note that the H column densities in Table 1 imply  $A_V = 0.63 - 0.87 \text{ mag}$  for the  $N_H/A_V$  ratio of  $1.87 \times 10^{21} \text{ cm}^{-2}$ , i.e.  $E_{B-V} = 0.20 - 0.28$  assuming  $R_V = 3.1$ . This range is in good agreement with the  $E_{B-V} = 0.19$  value computed by comparing the value  $(B - V) = -0.04$  of 2dFS 3831 (Massey 2002) with the intrinsic value  $(B - V)_0 = -0.23$  of a B0-0.5III star (Wegner 1994) given the uncertainties on the photometry and spectral type (see section 3 for the optical spectroscopy of 2dFS 3831).

### 2.2 Timing Analysis

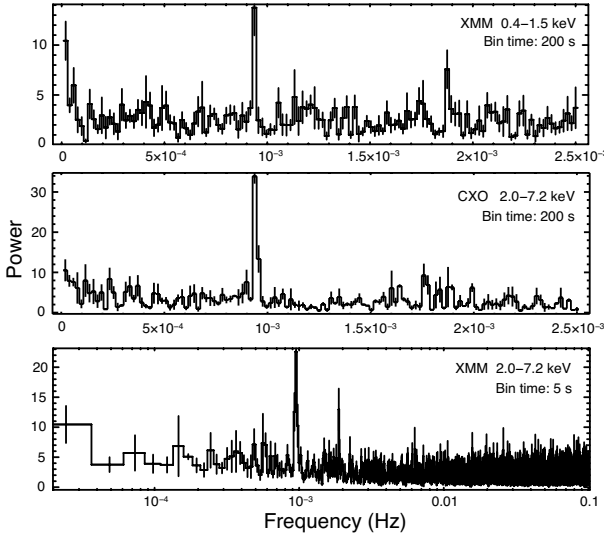
The photon arrival times were corrected for the solar system barycenter. We searched for pulsations in the X-ray light curves in the soft and hard energy bands (0.4 keV–1.5 keV, 2.0 keV–7.2 keV) and a total energy band (0.4 keV–7.2 keV), using fast Fourier transform and light-curve folding techniques as implemented in the timing analysis software *xrmos*.

Figure 2 shows the inferred *Chandra* and *XMM-Newton* power density spectra in the soft and hard energy bands with a clear peak at a frequency of  $9.4 \times 10^{-4} \text{ Hz}$  ( $P = 1062 \text{ s}$ ). This coherent X-ray pulse period establishes the source as a binary X-ray pulsar. The pulse profiles folded with this period are shown in Figure 3.

The light-curves used to compute the *XMM-Newton* power

**Table 1.** Best-fit parameters of the spectral models. The code for the different components of each model is: “P” for power-law, “B” for blackbody, and “T” for optically thin thermal emission with SMC abundances.

Model	$N_{\text{H}}$ ( $10^{21} \text{ cm}^{-2}$ )	$\Gamma$	$A_{\text{powerlaw}}$ (phot $\text{keV}^{-1} \text{ cm}^{-2} \text{ s}^{-1}$ )	$kT$ (keV)	$A_{\text{blackbody}}$ ( $10^{39} \text{ erg s}^{-1} \text{ kpc}^{-2}$ )	$kT$ (keV)	$A_{\text{thermal}}$ ( $10^9 \text{ cm}^{-5}$ )	$\chi^2/\text{DoF}$
P	$1.18 \pm 0.06$	$0.746 \pm 0.011$	$(6.60 \pm 0.11) \times 10^{-5}$	...	...	...	...	1.30
PB	$1.48 \pm 0.12$	$1.185 \pm 0.022$	$(6.35 \pm 0.35) \times 10^{-5}$	$2.13 \pm 0.05$	$(1.11 \pm 0.20) \times 10^{-5}$	...	...	1.21
PT	$1.63 \pm 0.04$	$0.732 \pm 0.011$	$(6.48 \pm 0.12) \times 10^{-5}$	...	...	$0.589 \pm 0.032$	$2.60 \pm 0.32$	1.19
PBT	$1.35 \pm 0.12$	$0.767 \pm 0.027$	$(4.87 \pm 0.30) \times 10^{-5}$	$1.54 \pm 0.16$	$(4.5 \pm 0.9) \times 10^{-6}$	$0.648 \pm 0.029$	$2.80 \pm 0.30$	1.07

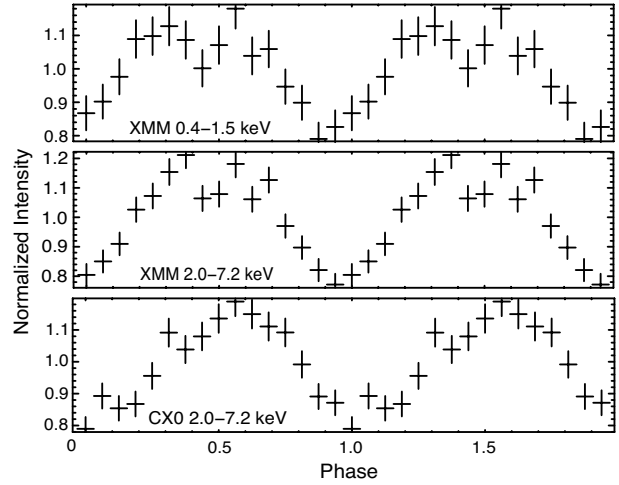
**Figure 2.** *XMM-Newton* and *Chandra* power density spectra in the soft and hard energy bands for different bin times.

spectrum in the hard energy band, the *XMM-Newton* power spectrum in the soft energy band, and the *Chandra* power spectrum in the hard energy band were binned by respectively 5 s, 200 s, and 200 s. The 5 s bin time for one of these was chosen to make sure that a shorter pulse was not missed. No pulse was found in the soft band *Chandra* observations, possibly because the count rate is too low. Because of the softer response of the EPIC-pn camera, the pulse in the soft band is the most obvious in the light-curves obtained with this instrument.

Note that in addition to the pulse period, X-ray variability was also detected at a level of  $\sim 20\%$  peak-to-peak on a timescale of several days in both *XMM-Newton* and *Chandra* light-curves. Given that this variability does not appear regular and that the time sampling is very sparse, we do not analyse these variations further.

### 3 OPTICAL SPECTROSCOPY

From its X-ray position with subarcsecond precision from *Chandra* images, the optical counterpart to SXP 1062 is identified as 2dFS 3831 (Evans et al. 2004). We observed this star with the VLT FLAMES instrument (Pasquini et al. 2002) on 2010 October 25 as part of a spectroscopic survey of massive stars in NGC 602 complementing our X-ray observations. Spectra were obtained in the Medusa-fibre mode of FLAMES using the LR02 setting of the Giraffe spectrograph (3960–4564 Å,  $R=7000$ , e.g. Evans et al. 2011). Five pairs of 1800 s exposures were obtained. The standard

**Figure 3.** Pulse profiles folded with a period of 1062 s in different energy bands.

data processing (bias subtraction, fibre location, summed extractions, division by flat-field, wavelength calibration) was done using the ESO Common Pipeline Library FLAMES reduction routines (v.2.8.7). Additionally, heliocentric correction and subtraction of a median sky spectrum were performed (for details see e.g. Evans et al. 2011). The spectra from all the exposures were then normalized and merged. The 2dF spectra of this star were also retrieved. These two spectra cover the regions from  $\sim 3800$  to  $4900$  Å and  $\sim 6000$  to  $7000$  Å, with resolving powers of 1500 and 2500 respectively (Evans et al. 2004). Figure 4 shows the VLT FLAMES and 2dF spectra of 2dFS 3831. The VLT FLAMES spectrum has been smoothed and rebinned to an equivalent resolving power of  $R=4000$ .

A weak He II  $\lambda 4542$  absorption line is visible in the VLT FLAMES spectrum and there is a hint of a weak He II  $\lambda 4686$  line in the 2dF spectrum, but He II  $\lambda 4200$  is absent, suggesting a spectral type around B0–0.5 following the classification adopted by Evans et al. (2004).

Several characteristics attributable to a circumstellar disc indicate that 2dFS 3831 is a classical Be star. Fe II  $\lambda 4179$  and Fe II  $\lambda 4233$  emission lines typical of some early Be stars (e.g. Slettebak 1982) are visible in the VLT FLAMES spectrum. The H $\alpha$  emission seen in the 2dF spectrum (see the right panel in Fig. 4) is relatively strong with an equivalent width (EW) of  $\sim 23$  Å. There is significant H $\beta$  emission, plus emission in the core of the other Balmer lines (double-peaked in the VLT FLAMES spectrum) and apparent infilling of the He I absorption lines. Two Micron All Sky Survey (2MASS; Skrutskie et al. 2006) JHK<sub>s</sub> photometry also indicates a clear infrared excess when compared with expected colors for a

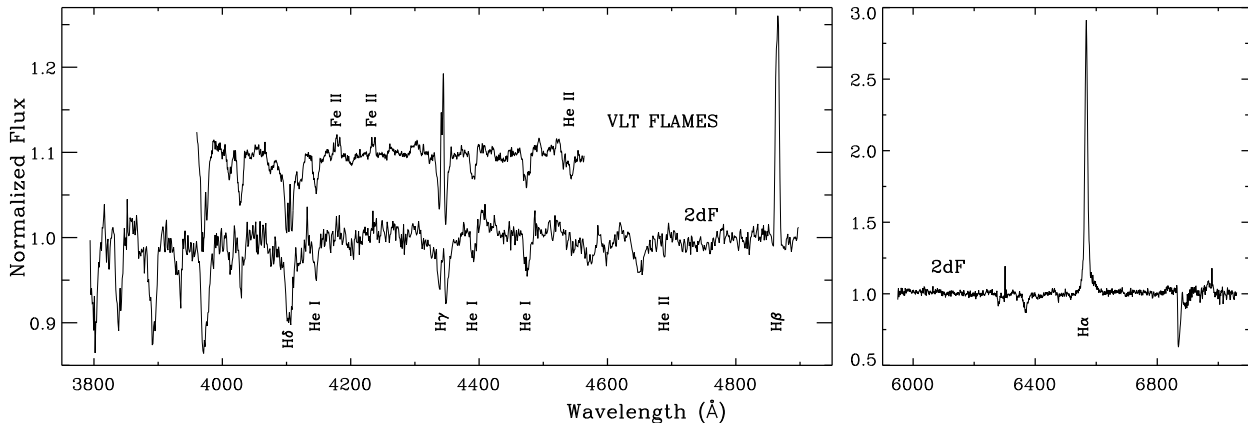


**Figure 4.** Optical VLT FLAMES and 2dF spectra of 2dFS 3831 with key spectral features identified. The VLT FLAMES spectrum is offset vertically.

B0-0.5 spectral type (Wegner 1994). The double-peaked emission in the Balmer lines is not due to oversubtraction of nebular features present in the median sky spectrum. Also, given the relative weakness of the nebular emission lines in the mean sky spectrum, the emission in the core of the Balmer lines is most likely dominated by circumstellar material and not by nebular contamination.

The observed magnitude ( $V=14.36$ ,  $B=14.32$ ; Massey 2002) and a range of reasonable extinction estimates (including both the interstellar and circumstellar components) lead to an absolute magnitude consistent with a B0-0.5 giant (Walborn 1972; Vacca et al. 1996). We thus determine the spectral type of 2dFS 3831 as B0-0.5(III)e+, where ‘+’ signifies the presence of Fe II. This corresponds to a typical effective temperature  $T_{\text{eff}} \sim 26000$  K and an evolutionary mass  $M \sim 15 M_{\odot}$  at SMC metallicity (cf. Trundle et al. 2007).

We estimated the radial velocity of 2dFS 3831 from the VLT FLAMES spectrum by fitting Gaussian profiles to the wings of H $\gamma$ , H $\delta$ , He I  $\lambda 4143$ , and He I  $\lambda 4388$ . The average of all measurements is  $167 \text{ km s}^{-1}$  with a standard deviation of  $13 \text{ km s}^{-1}$ . This is consistent with the mean velocity of massive stars in the SMC (Evans & Howarth 2008), and also with the gas velocities measured by Nigra et al. (2008) across the N90 H II region ionized by NGC 602A. Thus, we do not see any evidence that the HMXB acquired a high space velocity following the supernova explosion.

## 4 DISCUSSION

### 4.1 The properties of SXP 1062

SXP 1062 is only the third SMC X-ray pulsar with a spin period larger than 1000 s (Laycock et al. 2010). These slowly rotating pulsars are particularly interesting because they represent a challenge for the theory of spin evolution of a neutron star in a close binary system (e.g. Ikhshanov 2007).

According to the Corbet diagram for SMC Be-XRBs relating spin and orbital period (Corbet et al. 2009), we expect SXP 1062 to have a binary period of  $\sim 300$  days. Such a long orbital period is also expected from the  $P_{\text{orb}}$ -EW( $H\alpha$ ) diagram (Reig et al. 1997), from which our measured EW( $H\alpha$ ) suggests an orbital period of  $\sim 100$  days. Note however that the maximum EW( $H\alpha$ ) of the system, which probes the maximum size of the disc (and indirectly the orbital period), could be higher than our instantaneous measurement, so this period estimate should be taken as a lower limit.

SXP 1062 shares many characteristics with the class of persistent Be-XRBs (e.g. Reig 2011): a relatively low X-ray luminosity  $\sim 10^{34} - 10^{35} \text{ erg s}^{-1}$ , a slowly rotating pulsar with  $P > 200$  s, a relatively flat light curve with sporadic and unpredicted increases in intensity by less than an order of magnitude, and a lack of iron lines at  $\sim 6.4 \text{ keV}$  indicative of small amounts of material in the vicinity of the neutron star. A thermal excess of blackbody type, with a high temperature ( $kT > 1 \text{ keV}$ ) and a small emission area ( $R < 0.5 \text{ km}$ , consistent with a hot spot at the polar cap of the neutron star) has recently been suggested as a common feature of persistent Be-XRBs (La Palombara et al. 2009). Such a component is also identified in the X-ray spectrum of SXP 1062, for which we infer a size of  $\sim 0.4 \text{ km}$  for the blackbody source from our best-fit models (section 2.1).

### 4.2 The environment of SXP 1062

A shell nebula is detected around SXP 1062 in the Magellanic Cloud Emission-line Survey (MCELS; Smith et al. 1999)  $H\alpha$  image and in the higher resolution CTIO 4m MOSAIC (Muller et al. 1998)  $H\alpha$  image (see Figure 5). This shell is also detected in the MCELS [O III] image, but hardly in [S II]. We adopt below a distance modulus of 18.7. The shell is not uniform, with radii varying from  $75''$  at the sharp rim on the northeast to  $94''$  at the diffuse edge on the southwest. The peak surface brightness of the northeast rim is  $\sim 6 \times 10^{-17} \text{ ergs cm}^{-2} \text{ s}^{-1} \text{ arcsec}^{-2}$ , corresponding to an emission measure of  $30 \text{ cm}^{-6} \text{ pc}$ . The width of the rim suggests that the shell thickness ( $\Delta R$ ) is 5–10% of the shell radius ( $R$ ). The longest emitting length at the shell rim is  $2R[1 - (\Delta R/R)^2]^{1/2}$ ; thus, the rms density in the shell is  $1.3 \pm 0.3 \text{ H-atom cm}^{-3}$ . The gas mass in the shell is  $250 \pm 100 M_{\odot}$ . This large mass indicates that the shell gas must be dominated by interstellar material.

The shell morphology resembles supernova remnants (SNRs) in the Magellanic Clouds. The X-ray images also suggest that diffuse X-ray emission possibly associated with a SNR may be present in the vicinity of SXP 1062 (Oskinova et al., in preparation). As the shell mass is much larger than the typical supernova ejecta mass, we assume that the shell is a SNR in the Sedov phase. The kinetic energy in the shell would be  $\sim 30\%$  of the supernova explosion energy. Adopting a canonical explosion energy of  $10^{51} \text{ ergs}$ , the current shell kinetic energy is  $3 \times 10^{50} \text{ ergs}$ , and implies a shell expansion velocity of  $350 \pm 100 \text{ km s}^{-1}$  and an age of  $0.4(R/V) = (2-4) \times 10^4 \text{ yr}$ . This age is much larger than the cooling timescale of this low density gas, justifying an adiabatic shock for the Sedov phase. The



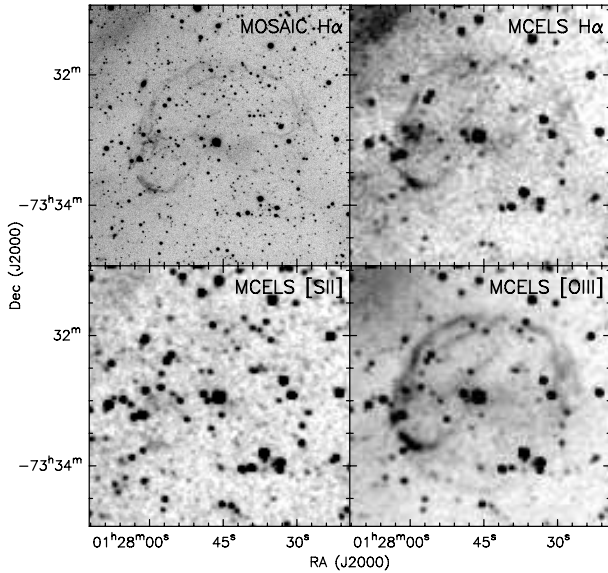


**Figure 5.** MOSAIC  $H\alpha$  image and MCELS  $H\alpha$ , [S II], and [O III] images of a region centered on the position of 2dFS 3831=SXP 1062 and showing the shell nebula detected around the target.

pre-shock interstellar gas density,  $1/4$  the shell density, is  $0.3 \pm 0.1$  H-atom  $\text{cm}^{-3}$ , consistent with the low density expected in the SMC Wing. The bright [O III] emission can be easily produced by a  $350 \text{ km s}^{-1}$  shock (cf. Hartigan et al. 1987). The ionizing flux of the B0–0.5III star can easily photoionize the shell gas and its surrounding pre-shock medium; furthermore, the diffuse [O III] emission to the northeast exterior of the shell indicates the existence of a harsh radiation field; therefore, the ionization stage of the pre-shock medium may be too high to produce strong post-shock [S II] emission. We thus conclude that the shell nebula detected around SXP 1062 is most likely a SNR. The extent of the shell, which has not reached the NGC 602 region, and its young kinematic age suggest that this supernova event did not trigger the formation of NGC 602.

## 5 CONCLUSION

We reported the discovery of a Be-XRB, SXP 1062, containing one of the slowest rotating X-ray pulsars in the SMC. We suggest that the shell nebula detected around this object is a SNR. Its estimated kinematic age of  $(2 - 4) \times 10^4$  yr is probably the age of the pulsar. This is, to our knowledge, the first discovery of a pulsar associated with a supernova remnant in the SMC.

## ACKNOWLEDGMENTS

This study is based on observations obtained with *XMM-Newton*, an ESA science mission with instruments and contributions directly funded by ESA Member States and NASA, and the *Chandra* science mission. The software provided by the *Chandra* X-ray Center (CXC) in the application package CIAO and by the *XMM-Newton* in the package SAS was used. This research has made use of NASA's Astrophysics Data System Service and the SIMBAD database, operated at CDS, Strasbourg, France. We thank Frank Winkler for providing the SMC MCELS images. VHB acknowledges support from SUPA and NSERC. LMO. acknowledges support from the DLR grant 50 OR 0804. MAG is supported by

the MICINN grant AYA2008-01934 that includes FEDER funds. W.S. acknowledges support from the DAAD grant A/10/95420. The DFG grant OS 292/3-1 supported the project workshop. YHC, JSG, and RAG acknowledge the support of NASA grant SAO G00-11025X.

## REFERENCES

- Antoniou V., Zezas A., Hatzidimitriou D., Kalogera V., 2010, *ApJS*, 716, L140  
 Carlson L. R. et al., 2007, *ApJS*, 665, L109  
 Cignoni M. et al., 2009, *AJ*, 137, 3668  
 Coe M. J., Edge W. R. T., Galache J. L., McBride V. A., 2005, *MNRAS*, 356, 502  
 Corbet R. H. D., Coe M. J., McGowan K. E., Schurch M. P. E., Townsend L. J., Galache J. L., Marshall F. E., 2009, *A Massive Star Odyssey: From Main Sequence to Supernova*, 4, 361  
 Evans C. J., Howarth I. D., 2008, *MNRAS*, 386, 826  
 Evans C. J., Howarth I. D., Irwin M. J., Burnley A. W., Harries T. J., 2004, *MNRAS*, 353, 601  
 Evans, C. J., Taylor, W. D., Hénault-Brunet, V., et al. 2011, *A&A*, 530, A108  
 Gouliermis D. A., Quanz S. P., Henning T., 2007, *ApJS*, 665, 306  
 Haberl, F., & Pietsch, W. 2004, *A&A*, 414, 667  
 Harries T. J., Hilditch R. W., Howarth I. D., 2003, *MNRAS*, 339, 157  
 Hartigan, P., Raymond, J., & Hartmann, L. 1987, *ApJS*, 316, 323  
 Hutchings J., Cartledge S., Pazder J., 1991, *AJ*  
 Ikhsanov N. R., 2007, *MNRAS*, 375, 698  
 La Palombara N., Sidoli L., Esposito P., Tiengo A., Mereghetti S., 2009, *A&A*, 505, 947  
 Laycock S., Zezas A., Hong J., Drake J. J., Antoniou V., 2010, *ApJS*, 716, 1217  
 Massey P., 2002, *ApJ Supp.*, 141, 81  
 McGowan K. E. et al., 2007, *MNRAS*, 376, 759  
 Muller, G. P., Reed, R., Armandroff, T., Boroson, T. A., & Jacoby, G. H. 1998, *Proc. SPIE*, 3355, 577  
 Nigra L., Gallagher J. S., Smith L. J., Stanimirović S., Nota A., Sabbi E., 2008, *PASP*, 120, 972  
 Pasquini L. et al., 2002, *The Messenger*, 110, 1  
 Reig P., 2011, *Ap&SS*, 332, 1  
 Reig P., Fabregat J., Coe M. J., 1997, *A&A*, 322, 193  
 Schmalzl M., Gouliermis D. A., Dolphin A. E., Henning T., 2008, *ApJS*, 681, 290  
 Skrutskie M. F. et al., 2006, *AJ*, 131, 1163  
 Slettebak A., 1982, *ApJ Supp.*, 50, 55  
 Smith, R. C., & The MCELS Team 1999, *IAU Symp.* 190: *New Views of the Magellanic Clouds*, 28  
 Trundle C., Dufton P. L., Hunter I., Evans C. J., Lennon D. J., Smartt S. J., Ryans R. S. I., 2007, *A&A*, 471, 625  
 Vacca W. D., Garmany C. D., Shull J. M., 1996, *ApJS*, 460, 914  
 Walborn N. R., 1972, *AJ*, 77, 312  
 Webster B. L., Martin W. L., Feast M. W., Andrews P. J., 1972, *Nature*, 240, 183  
 Wegner W., 1994, *MNRAS*, 270, 229  
 Westerlund, B. E. 1964, *MNRAS*, 127, 429  
 Yokogawa J., Imanishi K., Tsujimoto M., Koyama K., Nishiuchi M., 2003, *PASJ*, 55, 161